We are IntechOpen,
the world's leading publisher of
Open Access books
Built by scientists, for scientists

4,800
Open access books available

122,000
International authors and editors

135M
Downloads

Our authors are among the

154
Countries delivered to

TOP 1%
most cited scientists

12.2%
Contributors from top 500 universities

WEB OF SCIENCE™

Selection of our books indexed in the Book Citation Index
in Web of Science™ Core Collection (BKCI)

Interested in publishing with us?
Contact book.department@intechopen.com

Numbers displayed above are based on latest data collected.
For more information visit www.intechopen.com

Hydrogen Adsorptivity of Bundle-Structure Controlled Single-Wall Carbon Nanotubes

Shigenori Utsumi[1] and Katsumi Kaneko[2]
[1]Department of Mechanical Systems Engineering,
Tokyo University of Science, Suwa
[2]Research Center for Exotic Nanocarbons,
Shinshu University
Japan

1. Introduction

Hydrogen (H_2) gas is an ideal clean fuel, because H_2 emits only water on burning and the energy content per unit mass is much greater than that of hydrocarbon fuels (Gregory & Oerlemans, 1998). Using H_2 as a fuel has been expected to prevent global warming. To achieve the effective utilization of H_2 energy, the development of its efficient storage method is necessary. H_2 is supercritical gas at room temperature; the critical temperature of H_2 is 33 K. Thus, it is difficult to store large amount of H_2 at room temperature because the supercritical gas does not liquefy even under high pressures. Efficient adsorbents for H_2 storage have been actively studied to overcome this problem.

Single-wall carbon nanotube (SWCNT) is considered to be the most promising material which can contribute to construct a new sustainable chemistry (Iijima, 1991; Iijima & Ichihashi, 1993; Hirsch, 2002; Saito et al., 1998) and particularly a H_2 storage system, because SWCNT bundles have both of internal and interstitial nanospaces which strongly interact even with supercritical H_2 (Liu et al., 1999; Wang & Johnson, 2000; Seung & Young, 2000; Xu et al., 2007; Kim et al., 2007). One SWCNT consists of one graphene sheet rolling up. Thus, SWCNT is a special material referred to as "bi-surface nature material" because the whole carbon atoms are exposed to the both internal and external surfaces, each with different nanoscale curvatures of the SWCNT wall (Noguchi et al., 2007; Fujimori et al., 2010). A SWCNT has a huge geometrical surface area of 2630 m^2 g^{-1}, the same as graphene. The effective surface area of SWCNTs for molecules varies with its tube diameter and the target molecular size. In addition to the large surface area, the differences between surfaces with positive and negative curvature can be exploited to establish unique material science and technology. Ordinary SWCNTs associate to form an ordered bundle structure through dispersion interaction, providing interstitial pore spaces surrounded by carbon walls with positive curvature, which are the strongest molecular sites. Therefore, bundled SWCNTs have considerable potential for application to gas storage, the stabilization of unstable molecules, quantum molecular sieving (Noguchi et al., 2010), specific reaction fields, gas sensing, electrochemical energy storage and so on (Banerjee et al., 2003; Arai et al., 2007).

However, when the interstitial pore width is just comparable to the size of a small molecule, the molecules preadsorbed in the interstitial nanospaces often block further adsorption, or the capacity of the interstitial pore spaces is too small compared with the internal nanospace capacity. Thus, it is necessary to establish a means for tuning the bundle structure for providing the larger capacity of internal and interstitial nanospaces with an optimum size for the target function, as the volume of the interstitial nanospaces at the strongest sites is too small.

Pillaring an SWCNT bundle is the best approach to control interstitial nanoporosity, realizing enhanced adsorptivity for supercritical gases such as H_2, and strengthening the specificity of the molecular recognition function (Abrams et al., 2007; Zhao et al., 2007). Here we report the simple preparation of fullerene (Kroto et al., 1985) (C_{60})-pillared SWCNT bundles by sonication of SWCNTs in a C_{60} toluene solution and the consequent enhancement of the supercritical H_2 adsorptivity of the SWCNTs (Arai et al., 2009). As C_{60} molecules have a conjugated π-electron structure similar to that of SWCNTs, the C_{60}-pillared SWCNT system can be regarded as a new nanocarbon. In fact, naphthalene-pillared SWCNT have pseudo-metallic property (Gotovac-Atlagić et al., 2010).

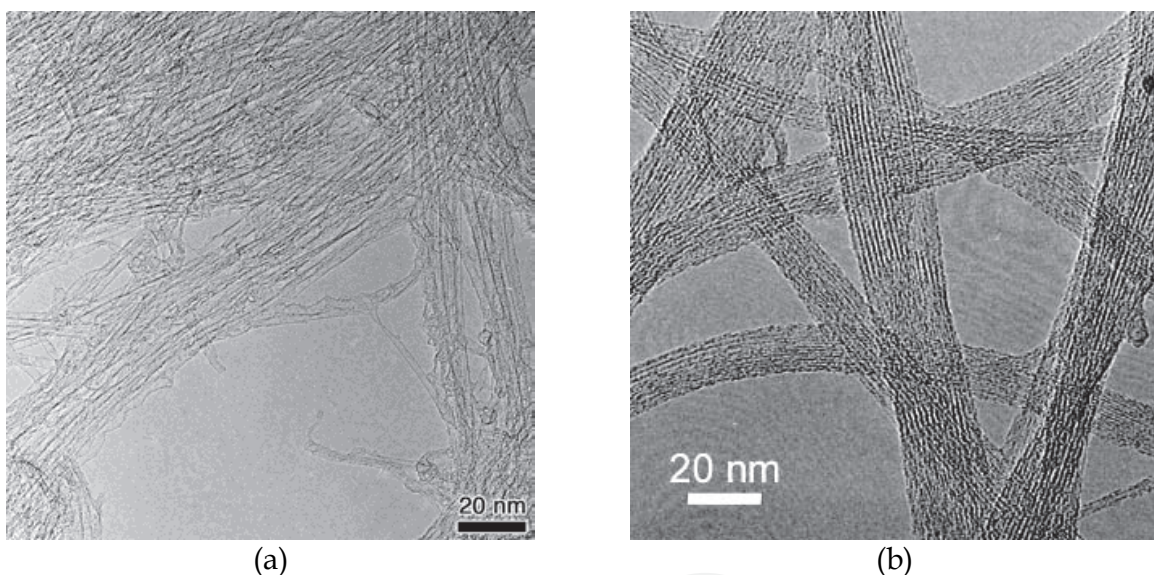| (a) | (b) |

Fig. 1. TEM images of SWCNT samples used. (a) Mutually isolated SG SWCNT prepared by the CVD method. (b) Well-bundled SWCNTs prepared by the laser ablation method.

Another approach to control the structure of SWCNT bundles is building up of the designed bundles from the isolated SWCNTs (Yamamoto et al., In press). Hata et al. succeeded to prepare mutually isolated SWCNTs of high purity using CVD method, stimulating interfacial researches on SWCNT (Hata et al., 2004). The transmission electron microscopy (TEM) image of SWCNT called as supergrowth SWCNT (SG SWCNT) is shown in Fig. 1a. SG SWCNT has the average diameter of 2.8 nm and the length of 1 mm order. Very recently, the authors evidenced that the monolayer of N_2 molecules adsorbed on the internal wall of the negative curvature of SWCNT is more ordered than that on the external wall of the positive curvature (Ohba et al., 2007). Thus, SWCNT has an explicit bi-surface nature for molecules, which should be applicable to develop intriguing and novel materials of multi-interfacial functions. If we control the bundle structure formation of the isolated SWCNTs induced by drying the SWCNTs dispersed in the solvent, many interstitial sites are formed

enough to adsorb supercritical H_2. The effect of surface tension of solvents, which are used to disperse SWCNTs, is focused on to control the bundle structure formation, since the SWCNTs in the bundle are bound by van der Waals force, that is, 27.9×10^{-3} and 22.1×10^{-3} N/m for toluene and methanol at 273 K, respectively.

In this chapter, we report the preparation of C_{60}-pillared SWCNT bundles and SWCNT bundles induced with capillary force-aided drying method, whose the supercritical H_2 adsorptivities are enhanced by C_{60}-pillaring and by the bundle formation.

2. Experimental section

2.1 Preparation and characterization of C_{60}-pillared SWCNT bundle

We used SWCNT samples prepared by the laser ablation of a graphite rod in the presence of Ni and Co (@ Institute of Research and Innovation: IRI) (Yudasaka et al., 1999; Kokai et al., 2000). The produced SWCNT was purified by the following method: SWCNT (200 mg) was added to a 15% hydrogen peroxide solution, and this solution was refluxed with a water bath at 373 K for 5 h to remove amorphous carbons. The residual catalysts of Ni and Co were removed by a 1 M hydrogen chloride solution. Then, SWCNT was filtrated, washed with doubly distilled water, and left at room temperature overnight. The TEM image of the purified SWCNT is shown in Fig. 1b. Characterization data for the purified SWCNT are shown in Fig. 2. Figure 2a shows thermogravimetry (TG) and differential thermogravimetry (DTG) curves measured in the N_2/O_2 flow. The estimated content of Co-Ni catalyst is about 8 wt%. X-ray diffraction (XRD) pattern shown in Fig. 2b measured using CuK_α exhibits a clear peak due to their well-ordered hexagonal bundle structure. The peak at 2θ=6.12° corresponds to 1.44 nm of interlayer distance d of SWCNT. Raman spectra in the radial breathing mode (RBM) band and G- and D-bands regions are shown in Fig. 2c. Very small peak at D-band indicates high-quality of the purified SWCNT. The tube diameter (d_{SWCNT}) is 1.37 nm, determined by the relation of $d_{SWCNT} = 248/w$, where w is the wavenumber of the RBM (Kataura et al., 1999). Closed SWCNT samples were used to clearly show the effect of C_{60}-pillaring. Figure 2d shows the N_2 adsorption isotherms of the purified SWCNT at 77K. The BET specific surface area is 337 m² g⁻¹, indicating that the purified SWCNTs were closed. For C_{60}-pillaring, we applied the methods used for the adsorption of organic substances on SWCNTs (Gotovac et al., 2007) and the preparation of peapod SWCNTs (Yudasaka et al., 2003). C_{60}-pillared SWCNTs were prepared by a simple sonication of SWCNT in C_{60} toluene solution with different concentrations. Purified SWCNTs (10 mg) were ultrasonically treated at 28 Hz for 6 h in C_{60}-dissolved toluene solutions of different concentrations up to 2.8 g L⁻¹$_{Toluene}$ in an ice storage. Then, the samples were stood for 24 h, filtrated, and dried in a vacuum at 333 K for 24 h. The amount of C_{60} on the SWCNT bundles was determined by the weight change of the samples before and after C_{60}-pillaring treatment. The C_{60}-pillared SWCNTs are designated as SWCNT-$C_{60}(x)$, where x is the amount in gram of C_{60} doped to 1 g of SWCNTs. Here, SWCNT-$C_{60}(0)$, which was ultrasonically treated in toluene without C_{60}, was also prepared for comparison.

The SWCNT-$C_{60}(x)$ samples were characterized with N_2 adsorption at 77 K, XRD, X-ray photoelectron spectroscopy (XPS), Raman spectroscopy, thermogravimetric analysis (TGA), and high resolution transmission electron microscopy (HR-TEM). The H_2 adsorptivity of the SWCNT-$C_{60}(x)$ samples was examined at 77 K by volumetric method. Samples were pre-evacuated at 423 K and 1 mPa for 2 h for the adsorption measurements of N_2 and H_2 at 77 K. TGA experiments were carried out in N_2 flow (100 ml/min) from ambient temperature to 1273 K at a rate of 5 K/min.
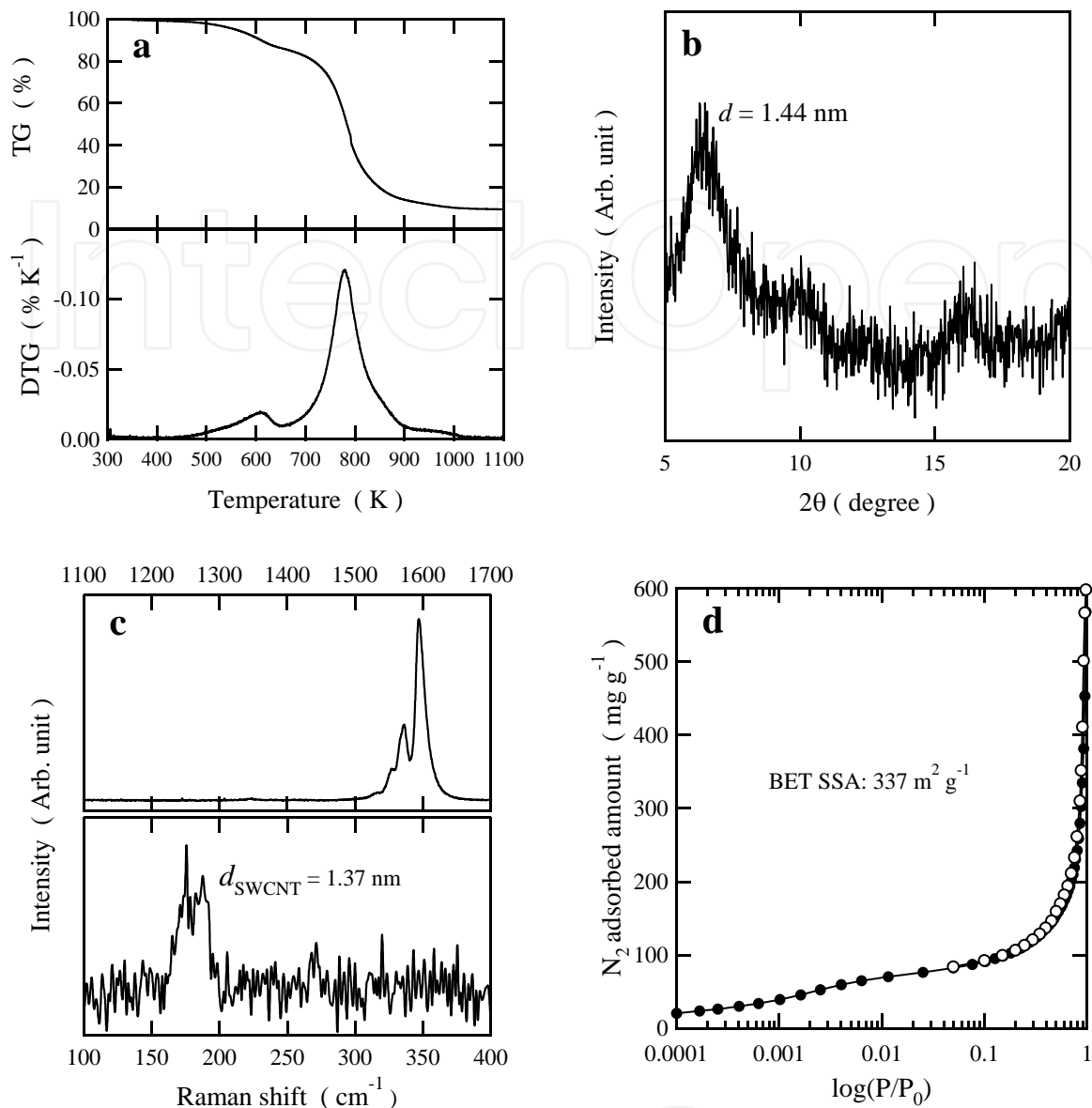
Fig. 2. Characterization data of purified SWCNT bundles prepared by laser ablation. (a) TG (upper)-DTG (bottom) curves. (b) XRD pattern of the superlattice of hexagonal SWCNT bundles measured using CuK_{α}. (c) G- and D-bands (upper) and RBM band (bottom) of Raman spectra. (d) N_2 adsorption isotherm at 77 K in terms of $\log(P/P_0)$.

2.2 Preparation and characterization of predominant bundle formation of isolated SWCNTs

The high purity isolated SWCNTs (SG SWCNTs) were produced by the CVD method (Hata et al., 2004). The SG SWCNTs were sonicated in toluene and methanol around 273 K for 12 h. Then, the SG SWCNTs in each solvent were filtrated and dried at 333 K for formation of the bundle structure by using the capillary force. The obtained SWCNT samples using toluene and methanol are denoted SWCNT/Tol and SWCNT/Met, respectively. The removal condition of residual toluene or methanol on SWCNT samples was determined by TGA before adsorption measurements. The nanopore structures of SWCNT/Tol and

SWCNT/Met were evaluated by N_2 adsorption measurements at 77 K after pretreatment at 423 K and 10^{-4} Pa for 2 h. The high pressure adsorption isotherms of supercritical H_2 were measured at 77 K by gravimetrical method after the pretreatment same as the N_2 adsorption measurement.

3. Results and discussion

3.1 C_{60}-pillared SWCNT bundle formation and its H_2 adsorptivity

The C_{60}-doped amount against the C_{60} concentration of the toluene solution (g $L^{-1}_{Toluene}$) is shown in Figure 3. The C_{60} uptake versus the C_{60} concentration curve has a step near 0.7 g g^{-1}_{SWCNT} of uptake and 0.5 g $L^{-1}_{Toluene}$ of the C_{60} concentration; the step indicates the formation of a stable structure between C_{60} and the SWCNTs. The uptake at the step closely corresponds to amount required for perfect filling of the interstitial spaces by C_{60} molecules, as estimated from the interstitial spaces in the model structure of an SWCNT bundle and the uptake of C_{60} for a trigonal arrangement as shown in Fig. 4 (Williams & Eklund, 2000).
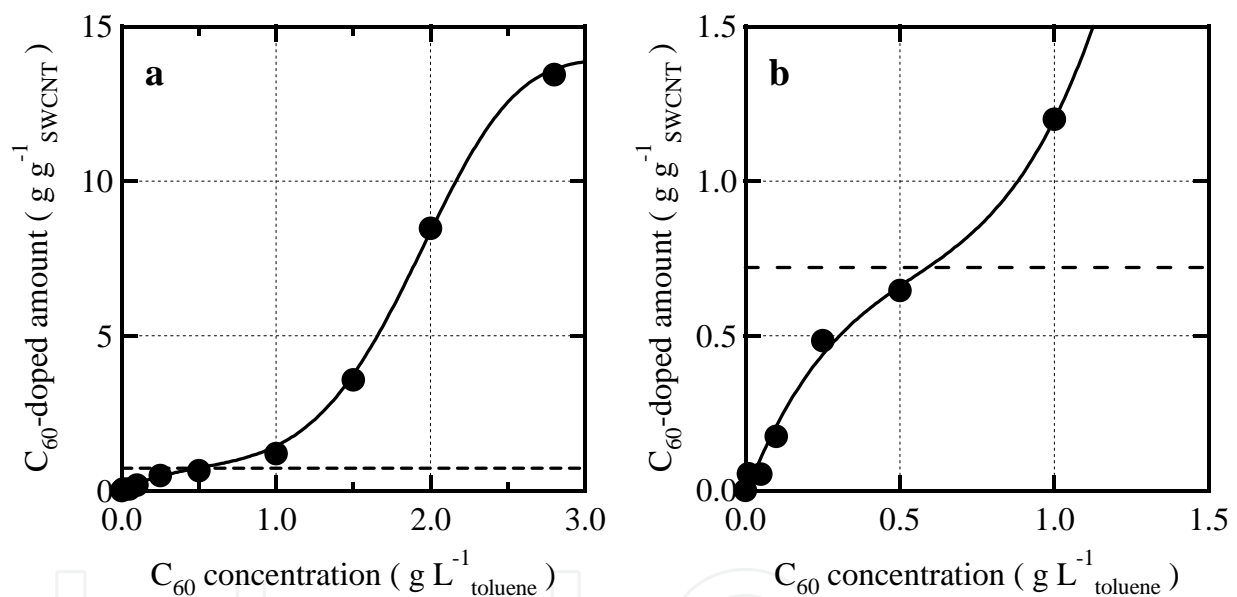

Fig. 3. C_{60}-doped amount on SWCNT bundles against the concentration of C_{60}-toluene solutions. (a) Relationship between the C_{60}-doped amount on 1 g of SWCNT samples (g g^{-1}_{SWCNT}) and the concentration of C_{60}-dissolved toluene. (b) Magnified view of Fig. 3a. The broken lines indicate the expected C_{60}-doped amount corresponding to perfect filling of the interstitial nanospaces with C_{60} in the model structure of C_{60}-pillared SWCNT bundles with hexagonal symmetry.

Figure 5 shows the N_2 adsorption isotherms of C_{60}-pillared SWCNT bundles. The N_2 adsorption amount was dramatically changed by C_{60}-pillaring treatment. The amount adsorbed on SWCNT-C_{60}(0.646) is the greatest. The adsorption isotherms of SWCNT-C_{60}(0.646) and SWCNT-C_{60}(1.68) have an extremely great uptake below P/P_0=0.1; the marked low pressure adsorption is more evidently observed in the isotherms of which abscissa is expressed by the log P/P_0. Accordingly the C_{60}-pillaring treatment increases the nanoporosity having a very strong interaction potential.
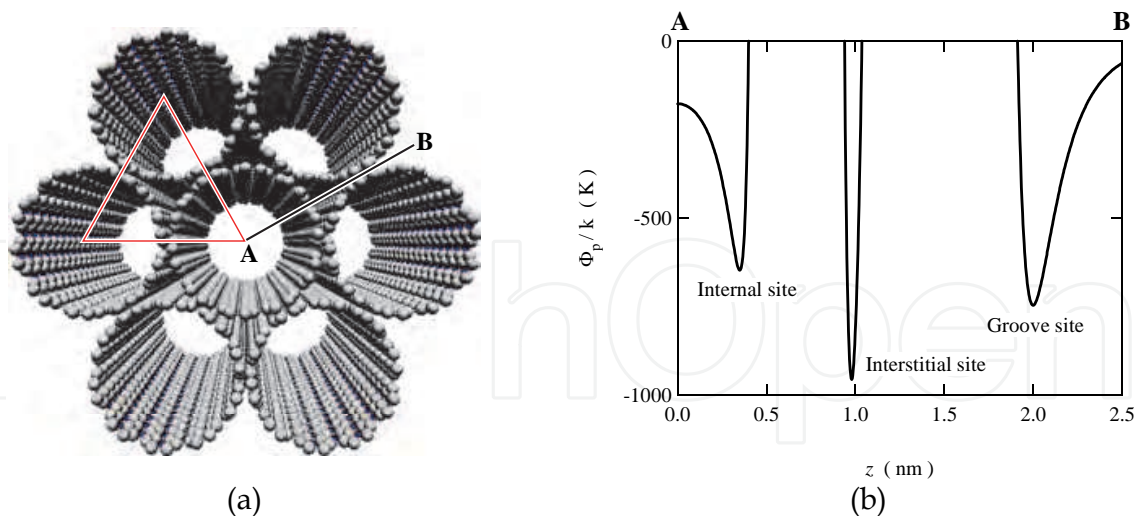
(a)   (b)

Fig. 4. Model structure and molecular potential field for hydrogen of an SWCNT bundle. (a) Typical SWCNT bundle composed of (10 10) SWCNTs having interstitial spaces for trigonal arrangement. (b) The potential field on the line connecting A and B in Fig. 4a is shown.
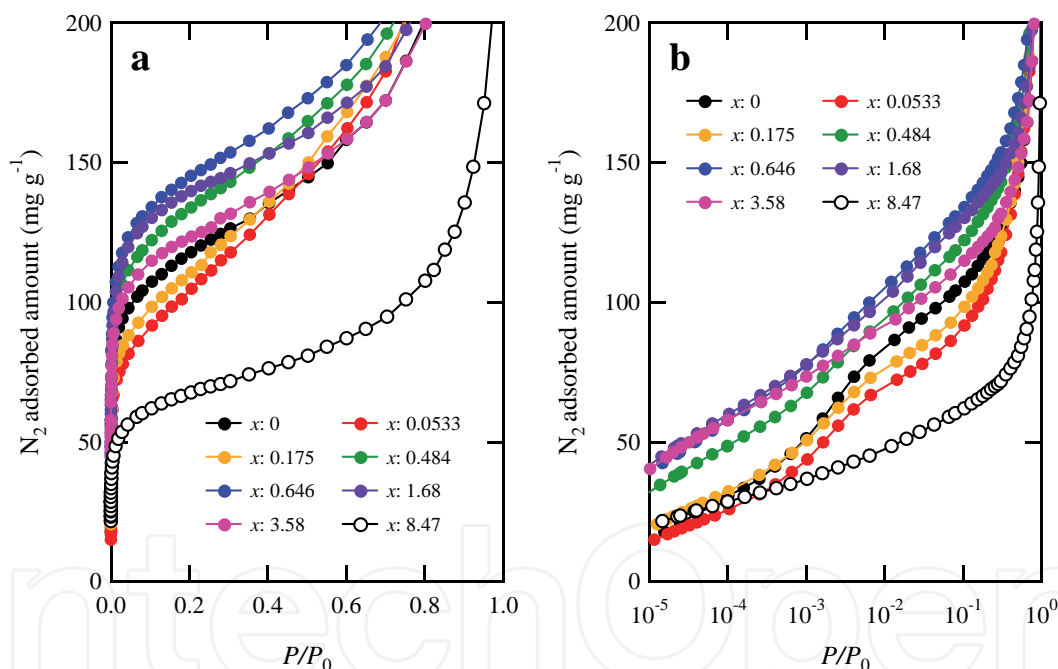

Fig. 5. N_2 adsorption isotherms of SWCNT-$C_{60}(x)$. The abscissas of **a** and **b** are expressed by N_2 relative pressure and the logarithm of N_2 relative pressure, respectively.

The stable structure, that is, SWCNT-$C_{60}(0.646)$, provides the maximum nanopore volume in N_2 adsorption measurements at 77 K. Figure 6 shows the relation between the nanospace volume and the C_{60}-doped amounts x (See Table 1 for detail). The nanospace volume of SWCNT-$C_{60}(0.646)$ is 0.15 cm³ g⁻¹, which is 1.36 times higher than that of SWCNT-$C_{60}(0)$. Hence, SWCNT-$C_{60}(0.646)$ should have the optimum C_{60}-pillared structure for the acceptance of molecules in the interstitial nanospaces expanded by C_{60}-pillaring. A C_{60} concentration higher than 1.0 g L⁻¹$_{Toluene}$ should induce further C_{60}-pillaring and coating of the external surface of the SWCNT bundle, thus reducing the nanopore volume.
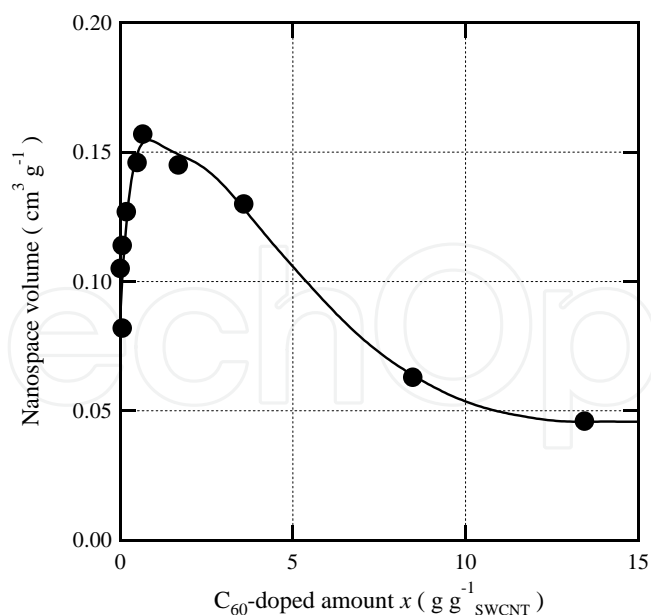
Fig. 6. Nanospace volume of C_{60}-pillared SWCNT as a function of the C_{60}-doped amounts x.
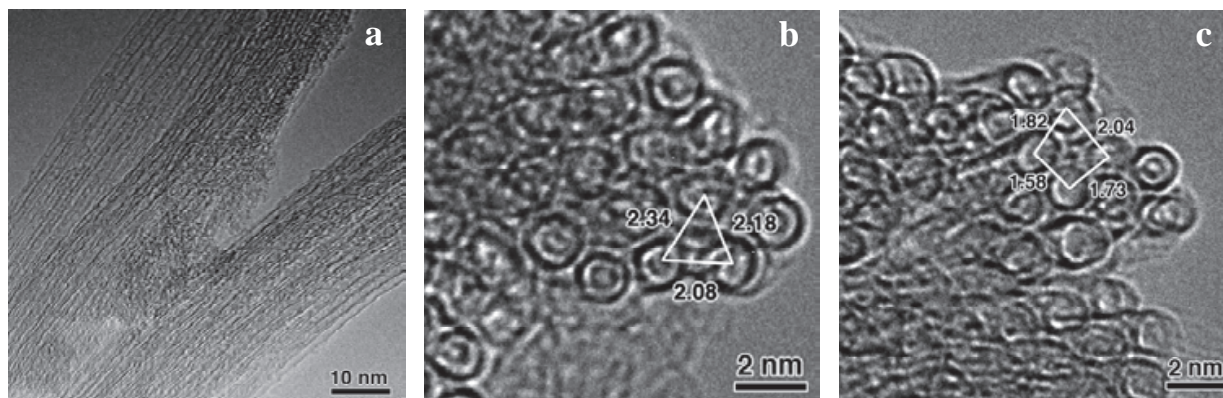

Fig. 7. TEM images of SWCNT-C_{60}(0.646) which has the maximum nanopore volume. (a) Side view of a C_{60}-pillared SWCNT bundle. (b) Cross-section of an expanded hexagonal SWCNT bundle. (d) Cross-section of a distorted-tetragonal array SWCNT bundle.

Figure 7 shows HR-TEM images of the bundle structure of SWCNT-C_{60}(0.646), which should have the optimum structure to adsorb molecules. The wide-range observation (Fig. 7a) shows a well-aligned bundle sheet even after ultrasonic C_{60}-pillaring treatment in the toluene solution. The side-view observation (Fig. 7a) indicates that C_{60} molecules are present on the SWCNT surfaces and there are no peapod SWCNTs (i.e., C_{60} in the SWCNTs). Figure 7b,c shows cross sections of the SWCNT-C_{60}(0.646) bundle having expanded hexagonal and tetragonal arrays, respectively. The intertube distance of the expanded bundle is estimated to be ~2.2 nm, leading to an interlayer distance d'=1.9 nm for hexagonal symmetry and d''=1.8 nm for tetragonal symmetry, under the assumption of uniform bundle structure for each symmetry. The interlayer distances d' and d'' of the bundles of hexagonal and tetragonal superlattices of the C_{60}-pillared SWCNT bundle are 2.03 and 1.92 nm, respectively, according to geometrical evaluation, which were close to the values

determined from TEM, as shown in Fig. 8. Thus, SWCNT-C_{60}(0.646) should have a mixed C_{60}-pillared structure with both hexagonal and tetragonal symmetries.
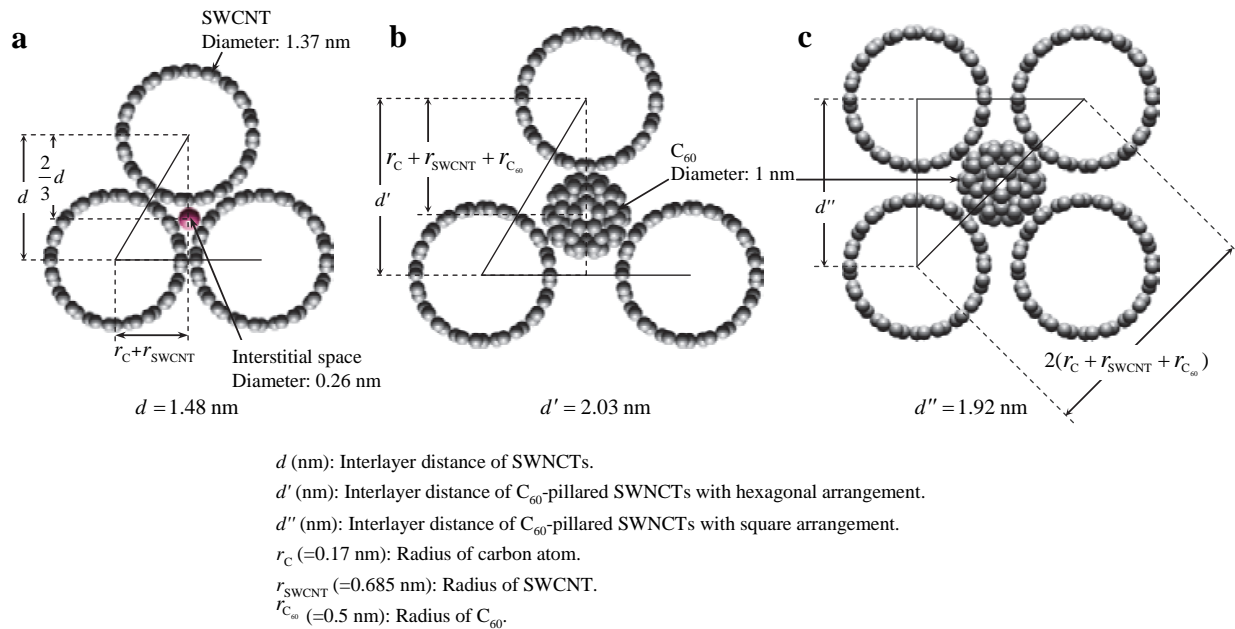

d (nm): Interlayer distance of SWNCTs.
d' (nm): Interlayer distance of C_{60}-pillared SWNCTs with hexagonal arrangement.
d'' (nm): Interlayer distance of C_{60}-pillared SWNCTs with square arrangement.
r_C (=0.17 nm): Radius of carbon atom.
r_{SWCNT} (=0.685 nm): Radius of SWCNT.
$r_{C_{60}}$ (=0.5 nm): Radius of C_{60}.

Fig. 8. Structure models and evaluation of interlayer distances for plausible C_{60}-pillared SWCNT bundles. Geometrical derivation of the interlayer distance d=1.48 nm of an SWCNT bundle with hexagonal arrangement (a), the interlayer distance d'=2.03 nm of an expanded hexagonal C_{60}-pillared SWCNT bundle (b), and the interlayer distance d''=1.92 nm of a C_{60}-pillared SWCNT bundle with tetragonal array (c).

Figure 9 shows XRD patterns which support the above-mentioned C_{60}-pillared SWCNT structure. SWCNT-C_{60}(0), which was ultrasonically treated in toluene without C_{60}, gives an explicit peak at 2.81° (X-ray source: MoK$_\alpha$), corresponding to the interlayer distance (d=1.44 nm (experimental)) of a hexagonal lattice of SWCNT arrays (see Fig. 8a), whereas individual SWCNTs have no diffraction peak in the concerned diffraction angle-range. This peak is weakened by the C_{60}-pillaring treatment and a broad peak appears around 2θ=2.0°. The new peak corresponds to an interlayer distance of ~2.0 nm, which is the average of 2.03 and 1.92 nm, derived from the TEM-derived two-structure models. Thus, XRD clearly indicates the formation of C_{60}-pillared SWCNT bundles. However, the pillared structure is not necessarily regular; hexagonal and tetragonal structures coexist, and therefore a broad superlattice peak is observed.

TGA data as shown in Fig. 10 revealed pillaring of C_{60} in the SWCNT bundles. Even SWCNT-C_{60}(0), which has no C_{60} exhibits a remarkable weight decrease ($\approx$ 10%) at 1200 K, which is caused by the elimination of amorphous carbon and oxygen functional groups. The weight decrease at high temperatures increases with increase in the C_{60}-doped amount x. The sample weight decrease is much less than the C_{60}-doped amounts, except in the region of low C_{60}-doped amount. The considerable weight decrease in the low C_{60} region is caused by the elimination of amorphous carbon and oxygen functional groups. On the other hand, only a part of the C_{60}-doped amounts adsorbed on the external surface of the SWCNT bundles can be eliminated in the high C_{60} region. This indicates that major C_{60} molecules inserted in the strong potential sites of interstitial pores cannot be eliminated.
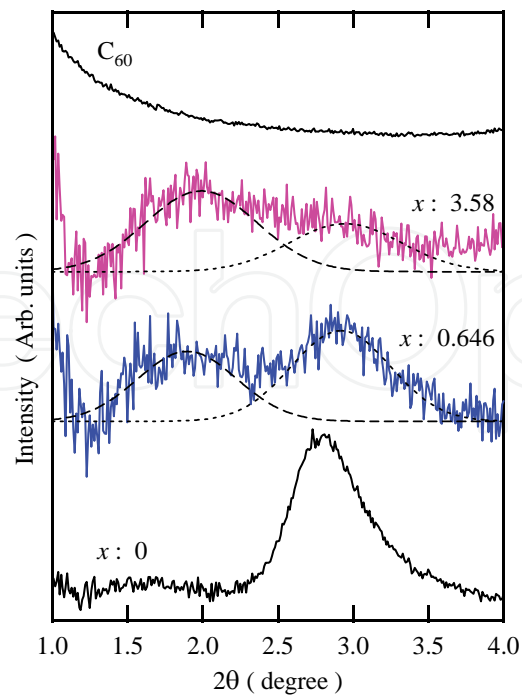
Fig. 9. XRD patterns of SWCNT-C$_{60}$(x) and C$_{60}$. The explicit peak of SWCNT-C$_{60}$(0) at 2.81°
evidences an ordered hexagonal SWCNT bundle. The peak position of broken lines almost
corresponds to the positions of the superlattice peaks of expanded hexagonal and tetragonal
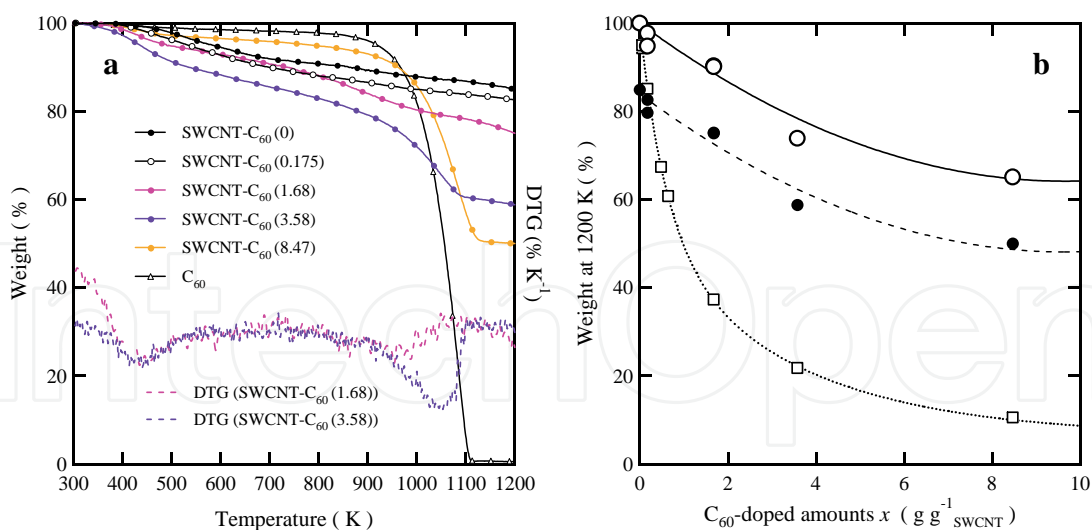array models of the C$_{60}$-pillared SWCNT bundle.

Fig. 10. TGA of SWCNT-C$_{60}$(x) samples and C$_{60}$. (a) TG and typical DTG (x: 1.68 and 3.58)
curves of SWCNT-C$_{60}$(x) and C$_{60}$. (b) Closed circles (●) indicate the weight percents (TG$_{1200\,K}$)
of the sample weight at 1200 K against the initial sample weight with C$_{60}$-doped amount.
Open circles (○) indicate the weight change at 1200 K of SWCNT-C$_{60}$, after correction of the
weight decrease of SWCNT itself. Open squares (□) correspond to the theoretical weight
decrease in percent of SWCNT-C$_{60}$(x) under the assumption that doped-C$_{60}$ is completely
sublimated.

Surface composition analysis with XPS also supports pillaring of C_{60} molecules in SWCNT bundles. Figure 11 shows the XPS spectra of C_{60}-pillared SWCNT bundles. XPS analysis of the C1s spectrum of SWCNT-C_{60}(0.646) by fitting with the C1s spectra of SWCNT and C_{60} shows the presence of 10% of C_{60} on the bundle surface, much less than the bulk content (39%) (Utsumi et al., 2007). XPS detects electrons only from surface layers in the order of 1 nm; predominant C_{60} molecules are not on the external surface of the SWCNT bundle, but inside of the SWCNT bundle as pillars. The absence of C_{60} on the bundle surface of SWCNT-C_{60}(0.646) is revealed by Raman spectroscopy shown in Fig. 12, which is also surface sensitive. The Raman peak for C_{60} at 1467 cm^{-1} appears only for the SWCNT-C_{60}(x) samples whose x is larger than 1.68 g g$^{-1}_{SWCNT}$ (Dresselhaus et al., 1996; Rao et al., 1997). Thus, all characterization results confirm that SWCNT-C_{60}(0.646) has a promising C_{60}-pillared structure with adequate nanoporosity.
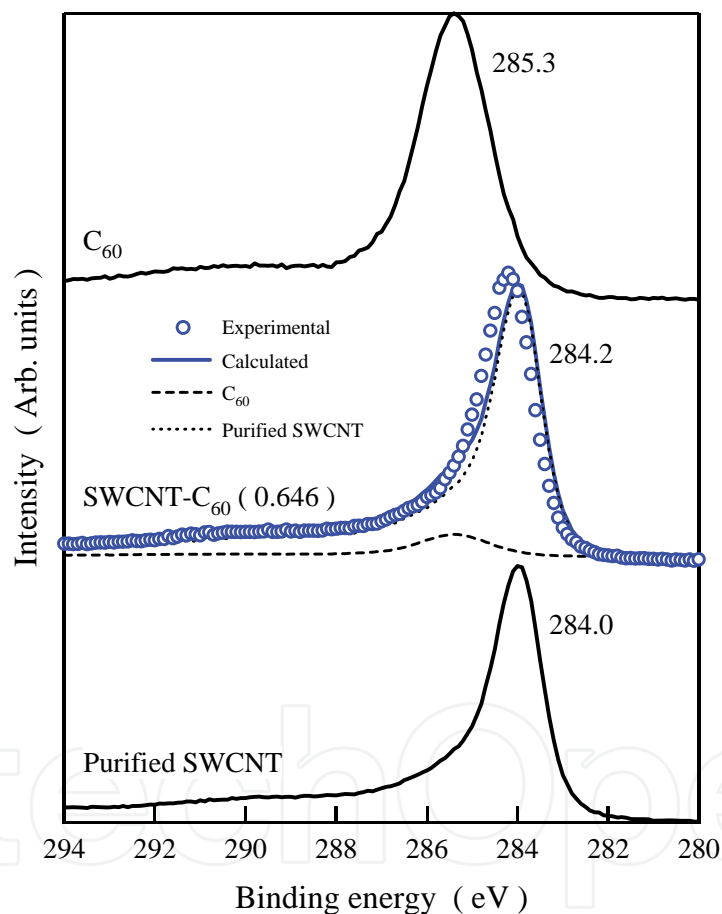

Fig. 11. C1s XPS spectra of SWCNT-C_{60}(x), SWCNT and C_{60}. The results of curve fitting (dotted line: purified SWCNT and broken line: C_{60}) for SWCNT-C_{60}(0.646) are shown. Estimated C_{60} amounts on the surface of SWCNT bundles from the XPS results are 10%.

The change in the interaction strength of the adsorption sites can be sensitively detected by supercritical H_2 adsorption. H_2 adsorption isotherms of SWCNT-C_{60}(x) at 77 K are shown in Fig. 13. For comparison, the isotherm of SWCNT-C_{60}(0) at 40 K is also shown. As the critical temperature of H_2 is 33 K, H_2 at 77 K and 40 K is supercritical, and thereby the adsorption of H_2 needs intensive assistance with interaction potential from solid nanospaces (Kaneko &
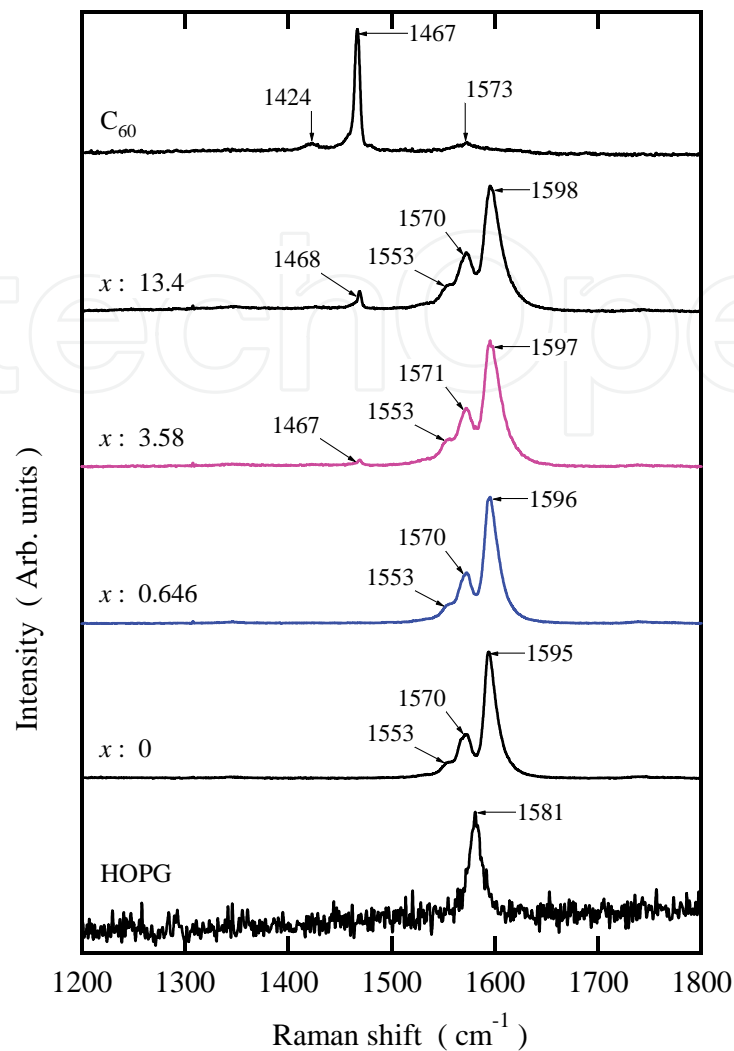
Fig. 12. Raman spectra of SWCNT-$C_{60}(x)$, SWCNT and C_{60}. Selective insertion of C_{60} in the bundle is confirmed by the absence of the Raman peaks of C_{60}.

Murata, 1997; Xu et al., 2007). As shown in Fig. 13, a large amount of H_2 can be adsorbed at enough low temperature such as 40 K ($\approx$ 1 wt% at 0.1 MPa), even though H_2 is supercritical. However, the H_2 adsorption amount at 77 K was less than the half of the amount at 40 K. H_2 adsorptivity of C_{60}-pillared SWCNT bundle was enhanced when the pillaring structure wasoptimum, while excessive C_{60}-doping reduced the H_2 adsorption amounts. Upward concave H_2 adsorption isotherms at relatively low pressure stems from the presence of strong adsorption sites, even for supercritical H_2. The adsorbed amounts per the weight and per the nanopore volume of SWCNT-$C_{60}(x)$ of supercritical H_2 at 77 K are plotted against the C_{60}-doped amount x, as shown in Fig. 14. H_2 adsorptivity of SWCNT-$C_{60}(x)$ per the sample weight markedly enhances the adsorption of H_2, providing almost twice the adsorption amount of SWCNTs in the low-pressure region, and 1.3 times higher in the ambient pressure region. On the other hand, H_2 adsorptivity of SWCNT-$C_{60}(x)$ per the nanopore volume remarkably decreased by C_{60}-pillaring. These results indicate that H_2 adsorptivity of SWCNT-$C_{60}(x)$ enhanced due to the increase in the nanopore volume, even though the interaction between the nanopore and supercritical H_2 were weakened.
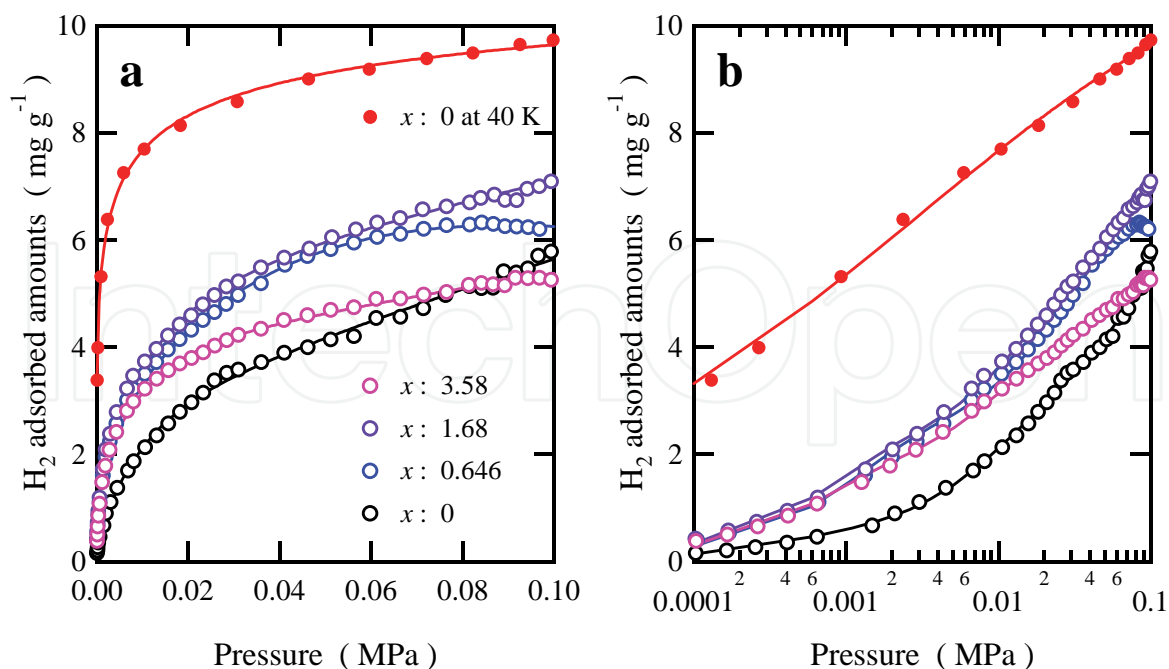
Fig. 13. H_2 adsorption isotherms of SWCNT-$C_{60}(x)$ at 77 K. For comparison, the isotherm of SWCNT-$C_{60}(0)$ measured at 40 K is also shown. The abscissas of **a** and **b** are expressed by the H_2 pressure and the logarithm of the H_2 pressure, respectively.
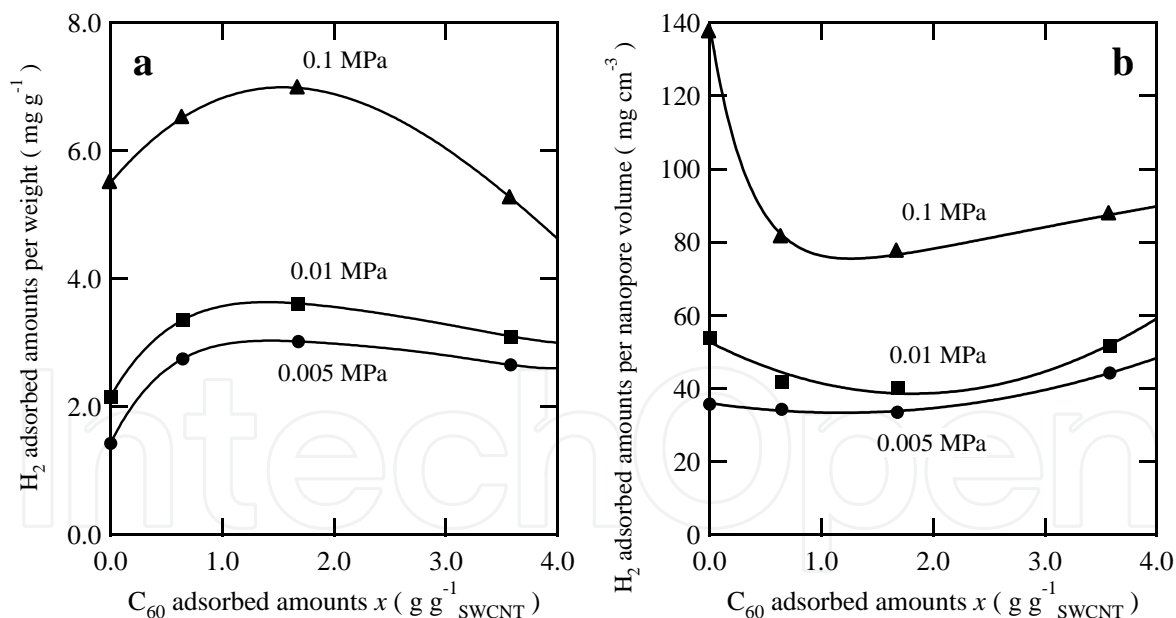

Fig. 14. H_2 adsorption amounts per the weight (a) and the nanopore volume (b) of SWCNT-$C_{60}(x)$ at 0.005 MPa (●), 0.01 MPa (■), and 0.1 MPa (▲) as a function of C_{60} adsorbed amount.

Supercritical gaseous molecules are concentrated in nanopores by the strong molecule-pore interaction and a supercritical gas adsorbed in nanopores is transformed into a quasi-vapor. The Dubinin-Radushkevich (DR) equation extended for a quasi-vapor supercritical gas is expressed in the terms of the quasi-saturated vapor pressure P_{0q} and the inherent nanopore volume V_L by

$$\left[\ln\left(\frac{V_L}{V}\right)\right]^{\frac{1}{2}} = \left(\frac{RT}{\beta E_0}\right)\left(\ln P_{0q} - \ln P\right), \tag{1}$$

where V is the nanopore volume at pressure P, E_0 the characteristic adsorption energy, and β the affinity coefficient. The isosteric heat of adsorption $q_{st,(\theta=1/e)}$ at the fractional filling θ of $1/e$ can be calculated using βE_0 and the enthalpy of vaporization ΔH_v at the boiling point from the relation of

$$q_{st,(\theta=1/e)} = \Delta H_v + \beta E_0. \tag{2}$$

The DR plot, that is, the plot of $[\ln(V_L/V)]^{1/2}$ versus $\ln P$ gives both values of P_{0q} under the nanopore field and $q_{st,(\theta=1/e)}$ (Kaneko et al., 1992; Kaneko & Murata, 1997). The typical DR plot for SWCNT-C_{60}(1.68) is shown in Fig. 15a, which exhibits a linear relationship. The isosteric heat of H_2 adsorption evaluated from the supercritical DR plot is shown in Fig. 15b. The isosteric heat is in the range of 9.5 to 9.7 kJ mol^{-1}, being almost constant regardless of C_{60}-pillaring. Thus, enhancement of the H_2 adsorptivity of C_{60}-pillared SWCNTs results from the increase in the nanospace volume. This value is much greater than the condensation enthalpy of H_2 molecules at the boiling point (~20 K; 0.22 kJ mol^{-1}) and the isosteric heat on the interstitial sites of (12, 12) SWCNT bundles (~9 kJ mol^{-1}) or on the slit pores of carbon (~8 kJ mol^{-1}) evaluated from Grand Canonical Monte Carlo simulation, indicating strong H_2 molecule-interstitial pore interaction in the C_{60}-pillared SWCNT bundles.
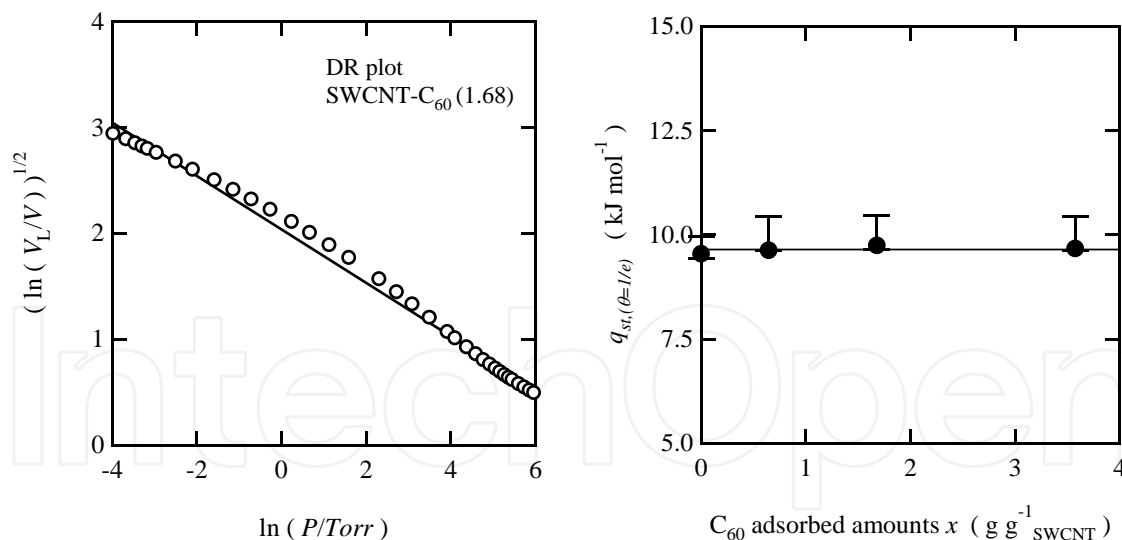

Fig. 15. Representative supercritical DR plot for SWCNT-C_{60}(1.68) and H_2 adsorption heat of SWCNT-C_{60}(x) derived from the supercritical DR plot as a function of C_{60} adsorbed amount.

3.2 Predominant bundle formation from isolated SG SWCNTs

Figure 16 shows the N_2 adsorption isotherms of SG SWCNT, SWCNT/Tol, and SWCNT/Met at 77 K. The N_2 adsorption isotherm of SG SWCNT is of IUPAC type II, showing that SG SWCNT is mutually isolated and the caps are closed. On the other hand, the isotherms of SWCNT/Tol and SWCNT/Met are close to IUPAC Type I, indicating the

presence of predominant micropores. The specific surface area (SSA) determined by the α_s method (Kaneko et al., 1998) is shown in Table 2. The SSAs of SWCNT/Tol and SWCNT/Met (750 m^2 g^{-1} and 760 m^2 g^{-1}) are considerably decreased by the sonication treatment, indicating the formation of the bundle structure with interstitial sites which are not accessible by N_2 molecules. SWCNT/Tol and SWCNT/Met should have enough bundle structure. Figure 17a shows the high pressure H_2 adsorption isotherms at 77 K, which are Langmuirian suggesting the presence of considerably strong interaction between H_2 and each SWCNT sample. Figure 17b shows adsorption isotherms expressed by the absolute H_2 amounts per the sample weight, which clearly show the formation of efficient surface for H_2 adsorption. Consequently, interstitial sites were efficiently introduced in the SWCNT bundle by the compression on drying with the aid of capillary force.
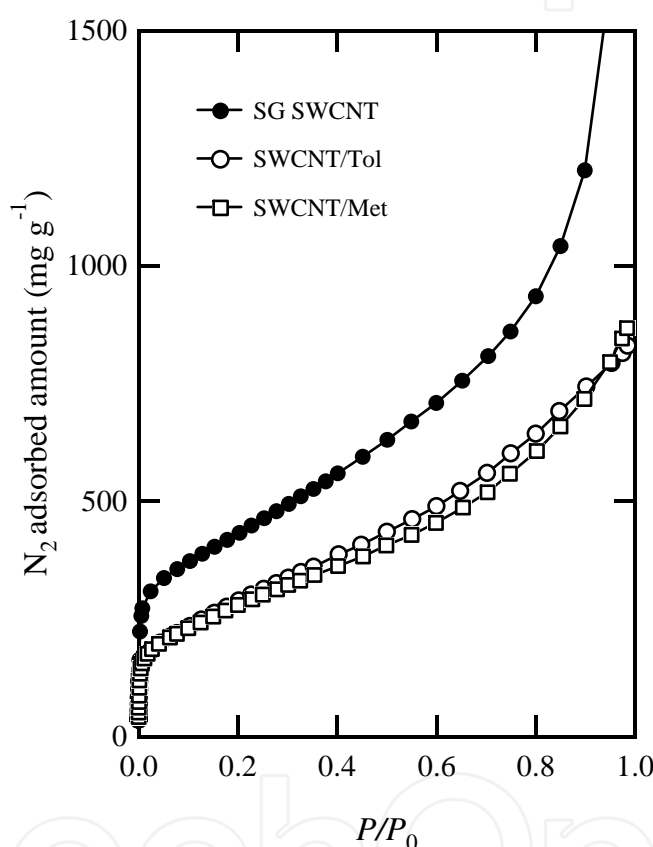

Fig. 16. N_2 adsorption isotherms of SG SWCNT (●), SWCNT/Tol (○), and SWCNT/Met (□) at 77 K.

Sample donation	SSA α_s	H_2 saturated adsorption amount	Quasi-saturated pressure	Heat of adsorption
	m^2/g	mg/g	MPa	kJ/mol
SG SWCNT	1,230	30	15	10.7
SWCNT/Tol	750	33	15	8.9
SWCNT/Met	760	29	13	9.0

Table 2. Parameters of bundle-structure controlled SG SWCNTs.
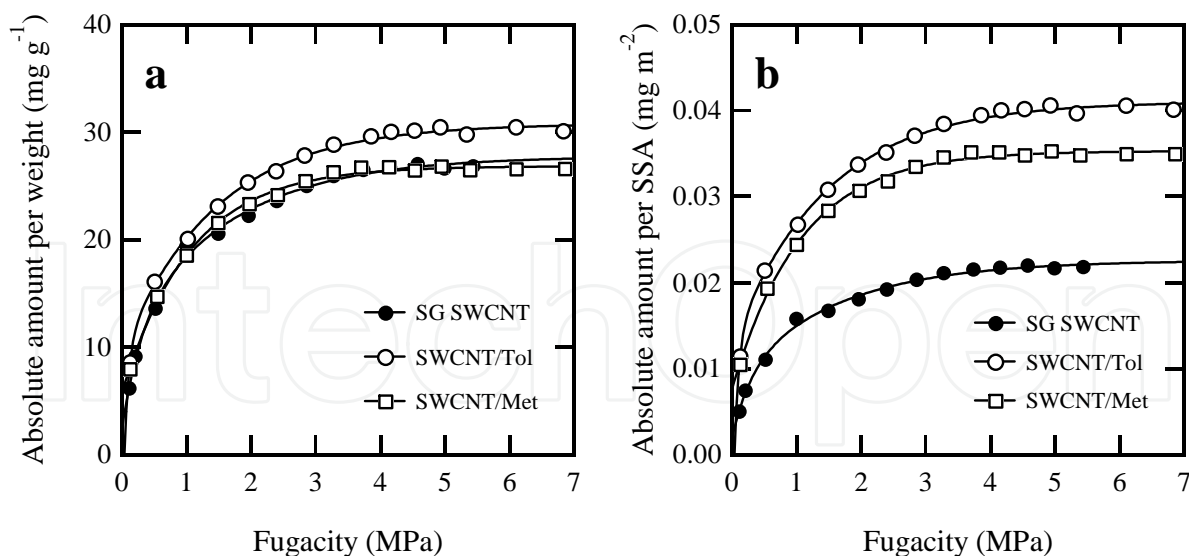
Fig. 17. High pressure H_2 adsorption isotherms of SG SWCNT (●), SWCNT/Tol (○), and SWCNT/Met (□). The vertical axes of **a** and **b** are expressed by the absolute H_2 amounts per the weight and per the specific surface area of the samples, respectively.

4. Conclusion

Two methods for tuning the bundle structure of SWCNT to enhance its H_2 adsorptivity were proposed; a one-step method for C_{60}-pillaring in SWCNT bundles by the cosonication of C_{60} and SWCNT in toluene and predominant bundle formation of the isolated SWCNTs by drying SWCNTs dispersed in toluene or methanol. C_{60}-pillared SWCNT with expanded hexagonal and distorted tetragonal arrays has enhanced H_2 adsorptivity, providing almost twice the adsorption amount of SWCNTs in the low-pressure region, and 1.3 times higher in the ambient pressure region. Isolated SWCNTs treated with toluene and methanol should make enough bundle structure by the compression on drying with the aid of capillary force, forming efficient surface for H_2 adsorption. These results indicate simple and promising tuning routes for SWCNT bundle structures, allowing the utilization of interstitial nanopore spaces for various fields, such as electrochemical, adsorption, sensor, and separation technologies.

5. Acknowledgment

6. References

Abrams, Z. R.; Ioffe, Z.; Tsukernik, A.; Cheshnovsky, O.; & Hanein, Y. (2007). A Complete Scheme for Creating Predefined Networks of Individual Carbon Nanotubes. *Nano Lett.*, Vol. 7, 2666-2671, ISSN 1530-6984.

Arai, M.; Utsumi, S.; Kanamaru, M.; Urita, K.; Fujimori, T.; Yoshizawa, N.; Noguchi, D.; Nishiyama, K.; Hattori, Y.; Okino, F.; Ohba, T.; Tanaka, H.; Kanoh, H.; & Kaneko, K. (2009). Enhanced Hydrogen Adsorptivity of Single-Wall Carbon Nanotube Bundles by One-Step C_{60}-Pillaring Method. *Nano Lett.*, Vol. 9, 3694-3698, ISSN 1530-6984.

Arai, M.; Kanamaru, M.; Matsumura, T.; Hattori, Y.; Utsumi, S.; Ohba, T.; Tanaka, H.; Yang, C.-M.; Kanoh, H.; Okino, F.; Touhara, H.; & Kaneko, K.; (2007). Pore characterization of assembly-structure controlled single wall carbon nanotube. *Adsorption*, Vol. 13, 509-514, ISSN 0929-5607.

Banerjee, S.; Kahn, M. G. C.; & Wong, S. S. (2003). Rational Chemical Strategies for Carbon Nanotube Functionalization. *Chem.-Eur. J.*, Vol. 9, 1898–1908, ISSN 0947-6539.

Dresselhaus, M. S.; Dresselhaus, G.; & Eklund, P. C. (1996). Raman Scattering in Fullerenes. *J. Raman Spectrosc.*, Vol. 27, 351-371, ISSN 0377-0486.

Fujimori, T.; Urita, K.; Ohba, T.; Kanoh, H.; & Kaneko, K. (2010). Evidence of Dynamic Pentagon-Heptagon Pairs in Single-Wall Carbon Nanotubes using Surface-Enhanced Raman Scattering. *J. Am. Chem. Soc.*, Vol. 132, pp. 6764–6767, ISSN 0002-7863.

Gotovac, S.; Honda, H.; Hattori, Y.; Takahashi, K.; Kanoh, H.; & Kaneko, K. (2007). Effect of Nanoscale Curvature of Single-Walled Carbon Nanotubes on Adsorption of Polycyclic Aromatic Hydrocarbons. *Nano Lett.*, Vol. 7, 583-587, ISSN 1530-6984.

Gotovac-Atlagić, S.; Hosokai, T.; Ohba, T.; Ochiai, Y.; Kanoh, H.; Ueno, N.; & Kaneko, K. (2010). Pseudometallization of single wall carbon nanotube bundles with intercalation of naphthalene. *Phys. Rev. B*, Vol. 82, 075136, ISSN 1098-0121.

Gregory, J. M. & Oerlemans, J. (1998). Simulated future sea-level rise due to glacier melt based on regionally and seasonally resolved temperature changes. *Nature*, Vol. 391, 474-476, ISSN 0028-0836.

Hata, K.; Futaba, D. N.; Mizuno, K.; Namai, T.; Yumura, M.; & Iijima, S. (2004). Water-Assisted Highly Efficient Synthesis of Impurity-Free Single-Walled Carbon Nanotubes. *Science*, Vol. 306, 1362-1364, ISSN 0036-8075.

Hirsch, A. (2002). Functionalization of Single-Walled Carbon Nanotubes. *Angew. Chem., Int. Ed.*, Vol. 41, 1853–1859, ISSN 1433-7851.

Iijima, S. (1991). Helical microtubules of graphitic carbon. *Nature*, Vol. 354, 56-58, ISSN 0028-0836.

Iijima, S. & Ichihashi, T. (1993). Single-shell carbon nanotubes of 1-nm diameter. *Nature*, Vol. 363, 603-605, ISSN 0028-0836.

Kaneko, K.; Ishii, C.; Kanoh, H.; Hanzawa, Y.; Setoyama, N.; & Suzuki, T. (1998). Characterization of porous carbons with high resolution α_s-analysis and low temperature magnetic susceptibility. *Adv. Colloid Interface Sci.*, Vol. 76-77, 295-320, ISSN 0001-8686.

Kaneko, K. & Murata, K. (1997). An analytical method of micropore filling of a supercritical gas. *Adsorption*, Vol. 3, 197-208, ISSN 0929-5607.

Kaneko, K.; Shimizu, K.; & Suzuki, T. (1992). Intrapore field-dependent micropore filling of supercritical N_2 in slit-shaped micropores. *J. Chem. Phys.*, Vol. 97, 8705-8711, ISSN 0021-9606.

Kataura, H.; Kumazawa, Y.; Maniwa, Y.; Umezu, I.; Suzuki, S.; Ohtsuka, Y.; & Achiba, Y. (1999). Optical Properties of Single-Wall Carbon Nanotubes. *Synth. Met.*, Vol. 103, 2555-2558, ISSN 0379-6779.

Kim, D. Y.; Yang. C.-M.; Yamamoto, M.; Lee, D. H.; Hattori, Y.; Takahashi, K.; Kanoh, H.; & Kaneko K. (2007). Supercritical Hydrogen Adsorption of Ultramicropore-Enriched Single-Wall Carbon Nanotube Sheet. *J. Phys. Chem. C*, Vol. 111, pp. 17448–17450, ISSN 1932-7447.

Kokai, F.; Takahashi, K.; Yudasaka, M.; & Iijima, S. (2000). Laser Ablation of Graphite−Co/Ni and Growth of Single-Wall Carbon Nanotubes in Vortexes Formed in an Ar Atmosphere. *J. Phys. Chem. B*, Vol. 104, 6777- 6784, ISSN 1520-6106.

Kroto, H. W.; Heath, J. R.; O'Brien, S. C.; Curl, R. F.; & Smalley, R. E. (1985). C_{60}: Buckminsterfullerene. *Nature*, Vol. 318, 162-163, ISSN 0028-0836.

Liu, C.; Fan, Y. Y.; Liu, M.; Cong, H. T.; Cheng, H. M.; & Dresselhaus, M. S. (1999). Hydrogen Storage in Single-Walled Carbon Nanotubes at Room Temperature. *Science*, Vol. 286, 1127-1129, ISSN 0036-8075.

Noguchi, H.; Kondo, A.; Noguchi, D.; Kim, D. Y.; Ohba, T.; Yang, C.-M.; Kanoh, H.; & Kaneko, K.; (2007). Adsorptive Properties of Novel Nanoporous Materials. *J. Chem. Eng. Jpn.*, Vol. 40, 1159-1165, ISSN 0021-9592.

Noguchi, D.; Tanaka, H.; Fujimori, T.; Kagita, T.; Hattori, Y.; Honda, H.; Urita, K.; Utsumi, S.; Wang, Z.-M.; Ohba, T.; Kanoh, H.; Hata, K.; & Kaneko, K. (2010). Selective D_2 Adsorption Enhanced by Quantum Sieving Effect on Entangled Single-Wall Carbon Nanotubes. *J. Phys.: Condens. Matter*, Vol. 22, 334027, ISSN 0953-8984.

Ohba, T.; Matsumura, T.; Hata, K.; Yumura, M.; Iijima, S.; Kanoh, H.; & Kaneko, K. (2007). Nanoscale Curvature Effect on Ordering of N_2 Molecules Adsorbed on Single Wall Carbon Nanotube. *J. Phys. Chem. C*, Vol. 111, 15660-15663, ISSN 1932-7447.

Rao, A. M.; Eklund, P. C.; Hodeau, J.-L.; Marques, L.; & Nunez-Regueiro, M. (1997). Infrared and Raman studies of pressure-polymerized C_{60}s. *Phys. Rev. B*, Vol. 55, 4766-4773, ISSN 1098-0121.

Saito, R.; Takeya, T.; Kimura, T.; Dresselhaus, G.; & Dresselhaus, M. S. (1998). Raman intensity of single-wall carbon nanotubes. *Phys. Rev. B*, Vol. 57, 4145–4153, ISSN 1098-0121.

Seung, M. L.; & Young, H. L. (2000). Hydrogen storage in single-walled carbon nanotubes. *Appl. Phys. Lett.*, Vol. 76, 2877-2879, ISSN 0003-6951.

Utsumi, S.; Honda, H.; Hattori, Y.; Kanoh, H.; Takahashi, K.; Sakai, H.; Abe, M.; Yudasaka, M.; Iijima, S.; & Kaneko, K. (2007). Direct Evidence on C−C Single Bonding in Single-Wall Carbon Nanohorn Aggregates. *J. Phys. Chem. C*, Vol. 111, 5572-5575, ISSN 1932-7447.

Wang, Q. & Johnson, J. K. (2000). Optimization of Carbon Nanotube Arrays for Hydrogen Adsorption. *J. Phys. Chem. B*, Vol. 103, 4809-4813, ISSN 1520-6106.

Williams, K. A. & Eklund, P. C. (2000). Monte Carlo simulations of H_2 physisorption in finite-diameter carbon nanotube ropes. *Chem. Phys. Lett.*, Vol. 320, 325-358, ISSN 0009-2614.

Xu, W.-C.; Takahashi, K.; Matsuo, Y.; Hattori, Y.; Kumagai, M.; Ishiyama, S.; Kaneko, K.; & Iijima, S. (2007). Investigation of hydrogen storage capacity of various carbon materials. *Int. J. Hydrogen Energy*, Vol. 32, 2504-2512, ISSN 0360-3199.

Yamamoto, M.; Itoh, T.; Sakamoto, H.; Fujimori, T.; Urita, K.; Hattori, Y.; Ohba, T.; Kagita, H.; Kanoh, H.; Niimura, S.; Hata, K.; Takeuchi, K.; Endo, M.; Rodrígues-Reinoso, F.; & Kaneko, K. (In press). Effect of nanoscale curvature sign and bundle structure on supercritical H_2 and CH_4 adsorptivity of single wall carbon nanotube. *Adsorption*, ISSN 0929-5607.

Yudasaka, M.; Ajima, K.; Suenaga, K.; Ichihashi, T.; Hashimoto, A.; & Iijima, S. (2003). Nano-extraction and nano-condensation for C_{60} incorporation into single-wall carbon nanotubes in liquid phases. *Chem. Phys. Lett.*, Vol. 380, 42-46, ISSN 0009-2614.

Yudasaka, M.; Kokai, F.; Takahashi, K.; Yamada, R.; Sensui, N.; Ichihashi, T.; & Iijima, S. (1999). Formation of Single-Wall Carbon Nanotubes: Comparison of CO_2 Laser Ablation and Nd: YAG Laser Ablation. *J. Phys. Chem. B*, Vol. 103, 3576- 3581, ISSN 1520-6106.

Zhao, Y.; Sugai, T.; Shinohara, H.; & Saito, Y. (2007). Controlling growth and Raman spectra of individual suspended single-walled carbon nanotubes. *J. Phys. Chem. Solids*, Vol. 68, 284-289, ISSN: 0022-3697.

Carbon Nanotubes - From Research to Applications

Edited by Dr. Stefano Bianco

Since their discovery in 1991, carbon nanotubes have been considered as one of the most promising materials for a wide range of applications, in virtue of their outstanding properties. During the last two decades, both single-walled and multi-walled CNTs probably represented the hottest research topic concerning materials science, equally from a fundamental and from an applicative point of view. There is a prevailing opinion among the research community that CNTs are now ready for application in everyday world. This book provides an (obviously not exhaustive) overview on some of the amazing possible applications of CNT-based materials in the near future.

How to reference

In order to correctly reference this scholarly work, feel free to copy and paste the following:

Shigenori Utsumi and Katsumi Kaneko (2011). Hydrogen Adsorptivity of Bundle-Structure Controlled Single-Wall Carbon Nanotubes, Carbon Nanotubes - From Research to Applications, Dr. Stefano Bianco (Ed.), ISBN: 978-953-307-500-6, InTech, Available from: http://www.intechopen.com/books/carbon-nanotubes-from-research-to-applications/hydrogen-adsorptivity-of-bundle-structure-controlled-single-wall-carbon-nanotubes

INTECH
open science | open minds